

Noninvasive Material Thickness Detection by Aerosol Jet Printed Sensors Enhanced Through Metallic Carbon Nanotube Ink

Joseph B. Andrews, *Student Member, IEEE*, Changyong Cao, Martin A. Brooke, *Senior Member, IEEE*, and Aaron D. Franklin, *Senior Member, IEEE*

Abstract—Demand for cheaper and more functional sensors continues to rise in an era when data can be used to improve health, safety, and efficiency in daily lives. In this paper, we present a fully printed sensor capable of noninvasive material thickness detection. By applying an oscillating signal between two millimeter-scale electrodes, the fringing electric field is measurably perturbed by a material placed directly on top of the electrodes, leading to a linearly varying capacitance with change in the material's thickness. We simulate this electric field perturbation and experimentally demonstrate the linear correlation between capacitance and overlying material thickness. Various parameters, from sensor size and structure to substrate and ink materials, are studied to optimize the performance of the printed sensors. Sensors made of metallic carbon nanotube ink yield the best sensitivity, exhibiting a capacitance change of 26 fF per mm thickness of rubber—ten times more sensitive than devices composed of silver nanoparticle ink. Finally, we demonstrate an effective application of the sensors in automobile tires. By applying the sensors directly beneath the tread (within the tire), mm changes in the tread depth are able to be detected in a 99% confidence interval. These findings provide a straightforward, low-cost approach for monitoring mm changes in material thickness using noninvasive, printed sensors applicable to innumerable Internet-of-Things (IoT) applications.

Index Terms—Aerosol jet printing, printed sensors, carbon nanotubes, material thickness detection, Internet-of-Things (IoT).

I. INTRODUCTION

PRINTED electronics is a burgeoning field that has been increasing in popularity in both academia and industry based on inherent low-cost and high manufacturability. Coupled with the Internet-of-Things (IoT) information revolution, printed electronic sensors have tremendous promise as a means to create large-area, economically feasible devices that are capable of gathering and transmitting valuable data [1]. In addition, printed electronics manufacturing is highly compatible with flexible substrates for applications where form factor is a crucial parameter [2]. So far, printed sensors have been shown to measure temperature [3], tactile pressure [4],

electrochemical markers [5] and many other parameters of interest [6]–[8]. Yet, advancements in printed electronics are anticipated to facilitate increasingly greater breakthroughs that will fuel the pervasive data collection needed to drive the future of the IoT.

Recently, nanomaterial inks have become of great interest in printed thin-film electronics due to their extraordinary electrical properties and solution process favorability [9]–[12]. Specifically, single-walled carbon nanotube (CNT) inks have led to many significant advancements in printed transistors and sensors as they offer a range of electrical properties, from semiconducting to metallic, and are resilient to thermal and mechanical stress [13]–[15]. Advancements in the solution-phase processing of CNTs have led to their commercial availability in various inks, making them highly relevant for use in printed electronics applications [16], [17]. In this work, we capitalize on the relatively high conductivity, high surface area-to-volume ratio, and solution processability of nanomaterials to create sensitive, low-cost, robust, and noninvasive material thickness sensors using silver/gold nanoparticle and metallic CNT (m-CNT) inks [18].

Material thickness sensors have a broad range of applications in the fields of manufacturing, safety, and healthcare [19]–[23]. In the healthcare industry, biological tissues have been measured using various methods including magnetically-driven lens actuators [19] and radiographic techniques [20]. However, a simpler, less expensive design could lead to more widespread use and help determine ailments ranging from skin disease to larynx cancer [21]. In the manufacturing industry, measuring paint film thickness for aircrafts is of importance for safety and economic reasons and could be reliably solved using a low-cost, noninvasive material thickness sensor [22]. Finally, a safety hazard that a material thickness sensor would directly address is in the monitoring of tread depth on automobile tires. As tire tread wears, manipulation and safety of a vehicle is greatly affected, which can lead to severe traffic accidents or crashes [23]. An array of low-cost, printed sensors capable of detecting the deterioration of the tire tread depth would be a major advancement for improving vehicle safety. Today's IoT environment allows for sensors to connect with devices to provide real-time data that enhances safety, function, and innumerable other factors. A tire tread depth monitor that can wirelessly communicate when the tire becomes unsafe would be significant advancement for IoT in the transportation and shipping industries.

Manuscript received April 6, 2017; accepted May 22, 2017. Date of publication May 31, 2017; date of current version June 23, 2017. This work was supported by the Fetch Automotive Design Group, LLC. The associate editor coordinating the review of this paper and approving it for publication was Dr. Amitava Chatterjee. (*Corresponding author: Aaron D. Franklin.*)

The authors are with the Department of Electrical and Computer Engineering, Duke University, Durham, NC 27708 USA (e-mail: aaron.franklin@duke.edu).

Digital Object Identifier 10.1109/JSEN.2017.2710085

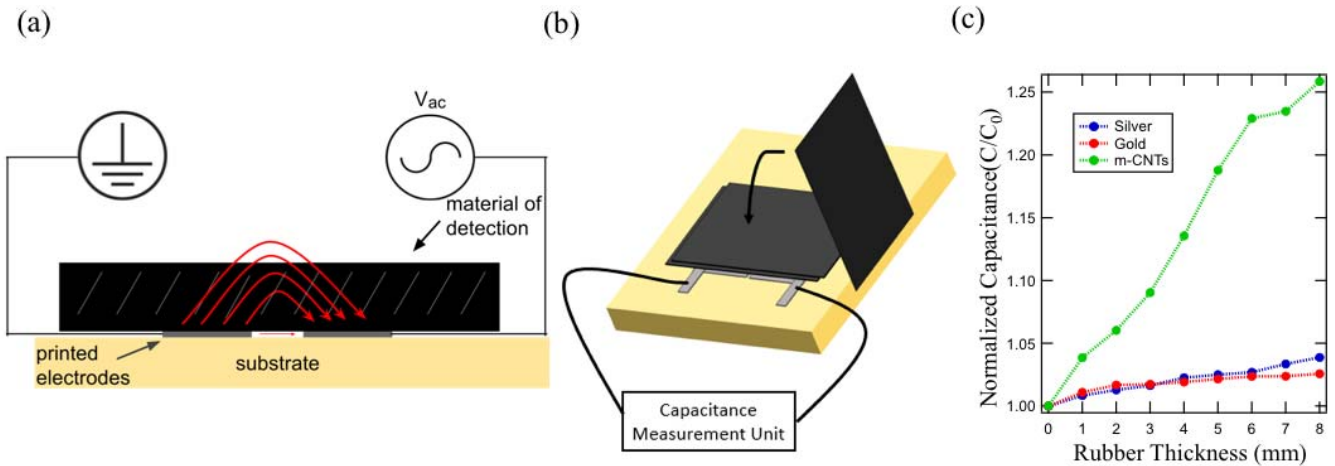


Fig. 1. Overview of printed sensor structure and operation as noninvasive material thickness detector. (a) Cross-sectional schematic of the printed sensor electrodes in the testing configuration, showing the fringing electric field that is perturbed by the overlying material. (b) Schematic showing how the measurement was accomplished, by placing 1 mm-thick rubber plies directly on top of the printed electrodes while monitoring the capacitance change using a CMU. (c) Comparison of sensitivity when measuring rubber thickness (plotted as normalized capacitance vs. rubber thickness) using three different inks: Ag and Au nanoparticles and m-CNTs. Sensor geometry was 5×5 mm with a $150 \mu\text{m}$ gap.

Previously, split ring resonators and other waveguides have shown the ability to measure both material thickness and dielectric properties through propagating electromagnetic fields. Most of these studies use an inductive measurement approach in which the material of detection will perturb the magnetic field of the system and ultimately change the resonant frequency of the split ring resonator [24]. However, it has also been shown that a capacitive approach can be used by placing rectangular waveguides directly abreast a dielectric material [25], [26]. While these previous works establish design concepts that can be built upon, they are prohibitive for many applications due to relatively high cost of manufacturing, especially when compared to a printing approach. Also, the above works focus on sensors on rigid substrates while compatibility with flexible substrates would be essential for many applications, such as in the automotive and aerospace industry where non-planar surfaces are common.

In this study, we demonstrate new sensors capable of noninvasively detecting the changes of material thickness. The sensors consist of two conducting electrodes printed adjacent to each other, as shown in Figure 1. Fringing electric fields propagate out of the electrode surface and through the medium of interest, thus being perturbed differently based on the thickness of the material on top of the electrodes, ultimately causing a measurable capacitance shift. All sensors in this work are fabricated using an aerosol jet printer, which is advantageous for printing a variety of different inks in an additive manufacturing fashion. Optimization of the sensors is carried out for a few factors, including sensor geometry, type of ink, and supporting substrate. The two congruent rectangular electrodes making up the sensor are adjacent to each other with a small gap between. The electrode sizes explored for optimization include 5×5 mm, 5×10 mm, and 10×10 mm, all with a gap of 1 mm. The gap between electrodes was also varied from 1 mm and $150 \mu\text{m}$, revealing a strong dependence of sensitivity on electrode spacing.

The two substrates used in the experiments were rigid glass slides and flexible Kapton (polyimide) films. Finally, various nanomaterial inks were explored, including Au nanoparticle, Ag nanoparticle, and metallic CNTs (m-CNTs).

II. EXPERIMENT

The sensors were printed using an aerosol jet printer (AJ300, Optomec Inc.). In the printing process, the nanomaterials were suspended in liquid solvents and ultrasonically atomized to form an aerosol mist. The mist was then carried by an inert nitrogen gas stream to the printing head and further aerodynamically focused at the nozzle using a sheath flow of N_2 gas to jet onto the substrate. This process allowed for resolution of printed line widths down to $10 \mu\text{m}$ and permitted a wide variety of inks to be used [27].

The substrates, either glass slides or Kapton films, were cleaned by sonication in acetone for 5 minutes, followed by sonication in IPA for 5 minutes, a rinse in DI water and finally drying using N_2 gas. The surfaces were then treated with oxygen plasma at 100 W for 4 minutes.

The silver nanoparticle ink (UT Dots, Inc. Ag40X) contained 40 wt % Ag dispersed in a xylene and terpinol solvent mixture (9:1 by volume). The Ag ink was printed into rectangular electrodes of various sizes on both the glass and the Kapton substrates. The silver nanoparticle samples were printed using a wide nozzle deposition head to enable higher throughput based on the relatively large printed sensor dimensions. This deposition head had a circular nozzle with a diameter of 3 mm. The sheath and atomizer flow rates were set to 200 and 150 sccm, respectively. The atomizer current needed to ultrasonically atomize the Ag ink was 430 mA. After printing, the Ag nanoparticles were sintered in an oven at 200°C for 1 h.

The gold nanoparticle ink (UT Dots, Inc., UTD-Au25) consisted of 25 wt % Au dispersed in a proprietary solvent mixture. The ink was mixed with a proprietary adhesion

promoter (BOL from UT Dots, Inc.) at a ratio of 100 to 1, respectively. The Au ink was also printed using the wide nozzle attachment with a diameter of 3 mm and the parameters for the sheath and atomizer flow were 150 and 130 sccm, respectively. The atomizer current needed to ultrasonically atomize the Au ink was 500 mA. After printing, the Au nanoparticles were sintered together in an oven at 280 °C for 1 h.

The m-CNT ink consisted of P3-SWNTs purchased from Carbon Solution, Inc. The nanotubes were dispersed as received in DI water at a 0.5 mg/mL ratio and ultrasonicated for 2 hours to form a uniform solution. Two layers of the m-CNT ink were printed using a 150 μm nozzle with sheath and atomizer flow rates of 35 and 25 sccm, respectively. The atomizer current needed to ultrasonically atomize the m-CNT ink was 370 mA. The printed m-CNT samples were finally placed in an oven at 150 °C to facilitate evaporation of any residual DI water.

The capacitance measurements were done using a B1500 Device Analyzer (Agilent Inc.). The measurements were carried out by sweeping an AC voltage of 50 mV on top of a fixed DC bias of 2 V across a range of frequencies from 10 kHz to 5 MHz.

At lower frequencies, the capacitance measurements were influenced significantly by random noise. The noise of the measurements was significantly reduced as the frequency approached 1 MHz. After 1 MHz, the capacitance rose sharply in a manner that was unrepeatably with multiple measurements. Therefore, the capacitance at 1 MHz was chosen for the analysis of the sensors.

The capacitance measurement unit attachment to the B1500 Device Analyzer directly measured the capacitance between the two electrodes by measuring the conductance (G) and admittance (Y). Using these values, the system calculates the capacitance between the printed electrodes by first calculating the susceptance (B) using equation 1 and then translating that into capacitance using equation 2, as follows:

$$|Y| = \sqrt{G^2 + B^2} \quad (1)$$

$$C_P = \frac{B}{2\pi f} \quad (2)$$

III. RESULTS AND DISCUSSION

To determine the effectiveness of the printed material thickness sensors, variations in size, ink, and spacing were studied. A consistent change in capacitance was observed based on changes to the thickness of overlying material directly atop the printed planar sensors across almost all studied variations. However, the overall response and level of linearity varied with each of the variables explored. We used two primary methods for determining the merit of each sensor configuration: change in capacitance vs change in rubber thickness and the square of the residuals (R^2) along a linear fit of the data. The former gives insight into the measurable sensitivity of the sensors and the latter provides information regarding the consistency across the interval of material thickness used in the experiments. Table 1 summarizes these two parameters for all devices studied. Note that all experiments of material

TABLE I
SUMMARY OF RESULTS

Ink	Size (mm)	Gap (μm)	Sub.	$\Delta C(\text{fF})/\Delta T$ (mm)	R^2
Ag	10 by 10	1000	Glass	1.05	0.967
Ag	5 by 10	1000	Glass	1.56	0.963
Ag*	5 by 5	1000	Glass	3.41	0.820
Ag	5 by 5	150	Glass	3.83	0.983
Ag	5 by 5	150	Kapton	2.82	0.993
Ag	5 by 5	150	Kap. Flex	7.87	0.721
Au	5 by 5	150	Glass	11.14	0.826
mCNT	5 by 5	150	Glass	26.45	0.981

* The change in capacitance per change in rubber thickness datum for the Ag nanoparticle based sensor with 5 by 5 mm electrodes and a gap of 1 mm was taken from a test different than the test shown in Figure 2. This is due to some changes in the setup between the datum in the table and the data included in Figure 2 that caused unrealistic variations.

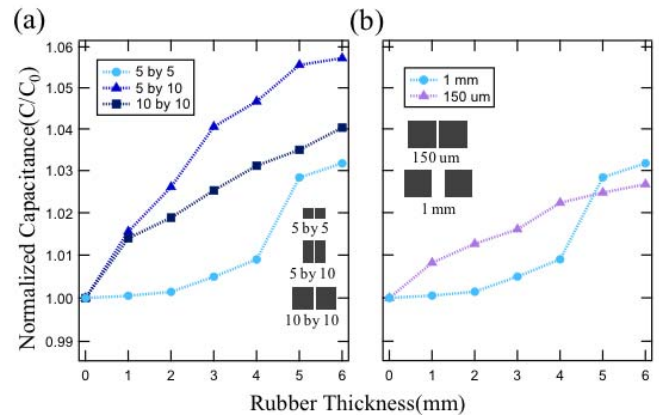


Fig. 2. Impact of printed electrode size and spacing on sensitivity. (a) Normalized capacitance change vs rubber thickness for three different electrode sizes (electrode separation = 1 mm), illustrated in the inset in mm. (b) Normalized capacitance vs. rubber thickness for two different electrode separation distances (electrode size = 5 by 5 mm).

thickness detection were performed using rubber films ~ 1 mm in thickness, added or removed to change overall thickness on top of the sensor.

The impact of sensor geometry using Ag nanoparticle ink is shown in Figure 2a. Out of the three electrode sizes with the same gap distance (1 mm), the 10 \times 10 mm and 5 \times 10 mm sensors outperformed the 5 \times 5 mm sensor in terms of low-noise linearity between capacitive response and material thickness; in other words, the R^2 value or the 5 \times 5 mm sensor is the lowest. One interesting note is that the linearity of the response is more directly related to the length of the sensor electrodes. This is attributed to the fact that the fringing field effect—which is responsible for the change in measured capacitance—is more reliant on the length as it defines the distance that will interact with the other electrode. This phenomenon is due to the operating principal of the fringing

electric field lines between the electrodes being perturbed by the dielectric material on top of them. The highest density of these lines, and the area in which these lines most heavily interact with the overlaid material, will occur close to the gap. It is imaginable that in further experiments one could lessen the width of the electrodes to something smaller all together to use less material and to create a higher resolution material thickness “map”. For example, if small area variations in material thickness over a large surface are of interest, smaller electrodes will allow for the sensing of these finer features, instead of allowing them to be averaged out. Similar works have applied the same principle with other sensors, specifically for pressure mapping [28].

It was hypothesized that the sensitivity would be dependent on the width of the gap between the two electrodes. This hypothesis is based primarily on the fact that the electric field between the two electrodes will be significantly stronger as the distance between the electrodes decreases. This will lead to a more measurable change in perturbation of said electric field by an overlaid material. To examine this variable, we compared the same 5×5 mm sensors with a 1 mm gap and a $150 \mu\text{m}$ gap. As shown in Figure 2b, the sensitivity of the sensor with the $150 \mu\text{m}$ gap is greatly magnified and has a stronger linear correlation when compared to the larger electrode sensors with a 1 mm gap. Thus, this geometry was used for all subsequent tests of different substrates and inks.

Next, the impact of the substrate that the sensors were printed on was studied, including the impact of substrate flexing during operation and is shown in Figure 3. The R^2 value and the sensitivity metric were approximately the same for the silver nanoparticle sensor printed on both substrates. This data is insufficient for performing a detailed analysis on the effect of substrate capacitance, except to state that the impact is minor between two vastly different substrates. Further analysis and experimentation would be needed to discover the direct correlation between substrate capacitance and overall sensitivity, but our results do show that the sensitivity of the sensor is robust across these two very different platforms.

The Kapton-supported sensor, when flexed over a curved base (radius of curvature = 5 cm) and the rubber placed conformably on top, showed improved performance with a much larger capacitance change per mm of rubber compared to that of the unflexed Kapton. However, there was also a more rapid saturation of the signal at only 4 mm of rubber. One possible explanation could be based on the decreased depth of the electric field lines. Because the depth of the fringing electric field lines is attenuated, the strength at which they interact with the overlaid material before a critical depth is exaggerated, leading to the higher change in capacitance over the initial 4 mm of rubber.

The effect of different nanomaterial inks on the overall sensitivity of the material thickness sensors was also considered. We found that sensors consisting of m-CNT ink had a 10x performance increase when comparing the change in capacitance vs mm change of rubber against the Ag nanoparticle-based sensor. Also, when imposed with a linear fit, the m-CNT sensors had a R^2 value of 0.981. This value indicates that the m-CNT-based sensors have a more

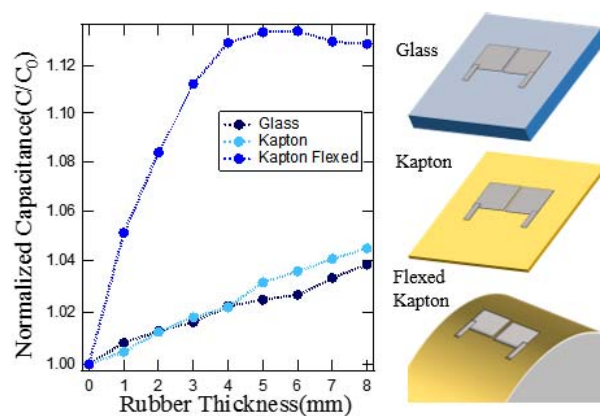


Fig. 3. Sensitivity and consistency over an 8-mm range in rubber thickness for identical Ag nanoparticle-based sensors printed on different substrates. Substrates included a glass slide, flat Kapton film and the same Kapton film flexed at a radius of curvature of 5 cm. Sensor geometry was 5×5 mm with a $150 \mu\text{m}$ gap.

linear response over the 8-mm range measured when compared to the Au sensors that exhibited an R^2 value of 0.826. The data, shown along with the SEM images in Figure 4, also has 99 % confidence intervals overlaid (derived from 10 serial capacitance measurements). The confidence intervals for the m-CNT ink are much tighter, indicating strong capacitance stability over numerous measurements.

The dependence of sensor performance on the electrode ink can be explained primarily by the thickness and the conductivity of the electrodes. The Au ink is the thickest and most conductive. This leads to a large portion of the electric field being expended between the sides of the two electrodes—laterally rather than out-of-plane. Hence, the mCNT ink performs better than the Ag and Au ink due to its nanometer level thickness, which allows for a higher concentration of the electric field out-of-plane, thus yielding higher sensitivity. This large surface area of the m-CNT film, coupled with the quantum confinement of electrons onto the outer area of the nanotubes themselves [9] and the incredible thinness of the electrodes fabricated through printing, results in an altogether more sensitive device.

To gain further insight into the impact of overlaid material on the fringing field lines of these sensors, a COMSOL simulation was carried out. Simulations displaying the electric field lines for 2 and 5 mm of overlaid rubber thicknesses are displayed in Figure 5. The higher permittivity of the rubber than that of the surrounding air leads to attenuation of the electric field lines. This is especially visible by comparing the field lines below the sensor (where the medium is kept as air in the simulation to highlight the contrast) to those above the sensor, where the rubber material is placed. For these simulations, the relative permittivity for the rubber was taken to be 14, and the electrodes were 5 mm by 5 mm with a spacing of 1 mm. Finally, a COMSOL simulation was completed to show the impact of having a thicker electrode (c), compared to the thinner electrodes modeled in (a) and (b). It is clearly visible through the simulation that the electric field is concentrated between the adjacent sides of the electrodes, leading to an electrical signal that is less perturbed by the overlaid material.

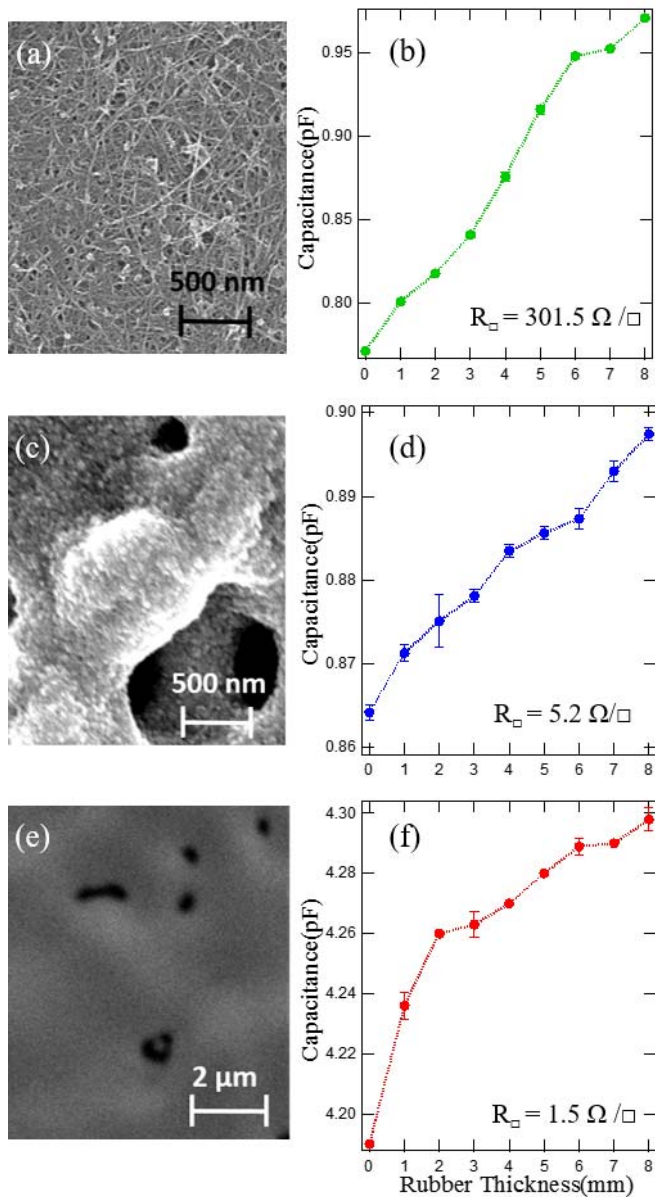


Fig. 4. Comparison of sensitivity and surface morphology for three different nanomaterial inks: Au and Ag nanoparticles and mCNTs. All sensors consisted of 5 by 5 mm electrodes with a separation distance of $150 \mu\text{m}$. (a) An SEM of the m-CNT film used for the electrodes in planar sensor geometry. (b) Plot of the capacitance (pF) vs overlaid rubber thickness (mm) with 99% confidence interval area bars. Sheet resistance of the m-CNT is also inset in the plot. (c) and (d) SEM and sensor data for the Ag nanoparticle electrode sensor. (e) and (f) SEM and sensor data for the Au nanoparticle electrode sensor.

Lastly, the operation of this sensor was demonstrated for use in detecting the rubber thickness of an automobile tire (tread depth). Traditionally manufactured tires have a steel mesh grid embedded within the rubber to improve stability and robustness. This metal grid presents a problem for the low-frequency capacitance measurements by screening a portion of field lines. However, hypothesizing that a sufficient portion of the field lines are still penetrating the metal grid, and that these field lines are still being attenuated by the changing rubber thickness, we developed an additional and more sensitive approach to detecting the attenuation. Rather than measuring capacitance, we measured the shift in resonant frequency

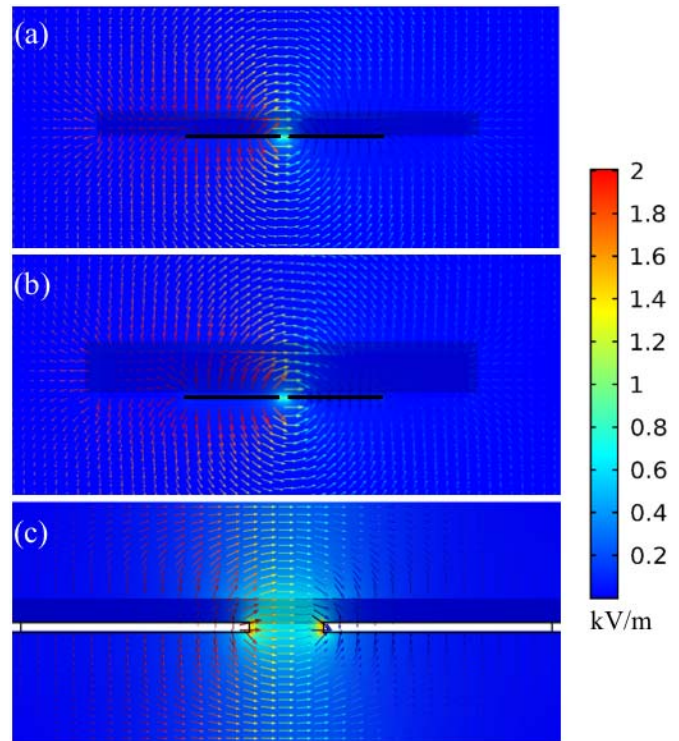


Fig. 5. Electric field distribution of the planar sensor calculated by COMSOL. The fringing electric field lines vary with the thickness of rubber overlaid on top of the electrodes. The rubber thickness used in the simulation was (a) 2 mm and (b) 5 mm, respectively. A sensor with thicker electrodes and a 2 mm thick rubber overlaid is shown in (c) and highlights the distribution of the electric field across the edges of the planar electrodes.

of a signal propagated between the two sensor electrodes—mechanistically the same as the capacitance approach but using a different signal and parameter to correlate to the material thickness (in this case, tread depth of a tire).

Using a vector network analyzer to provide a high frequency excitation signal on one electrode, the reflected signal was monitored on the adjacent electrode. The sensor used for this demonstration was a fully optimized “hybrid” sensor that consisted of a bottom layer of printed silver nanoparticles and a top layer of printed m-CNTs. This structure would comprise the significant advantages of both inks: high conductivity from the silver ink to distribute the field across the electrode and high surface-to-volume ratio of the m-CNTs to enhance sensitivity. The sensor was placed within the inner well of an automobile tire (beneath the tread portion of the tire) and an initial measurement was taken. Then, 1 mm thick rubber films were sequentially added on top of the tire while reflected signal measurements were taken in-between each addition. The results, with 99% confidence intervals, are plotted in Fig. 6, along with a photograph of the sensor used inside the tire. There was a linear correlation between the reflected signal at 487 MHz and the incremental change in tread depth via the added rubber pieces. In order to identify the operating frequency, the S11 response was monitored across a swept frequency range of 100 MHz to 1 GHz. From this sweep, two resonant peaks were identified, one at approximately 190 MHz and one at approximately 510 MHz. The second resonance proved to be highly sensitive to overlaid rubber material, and

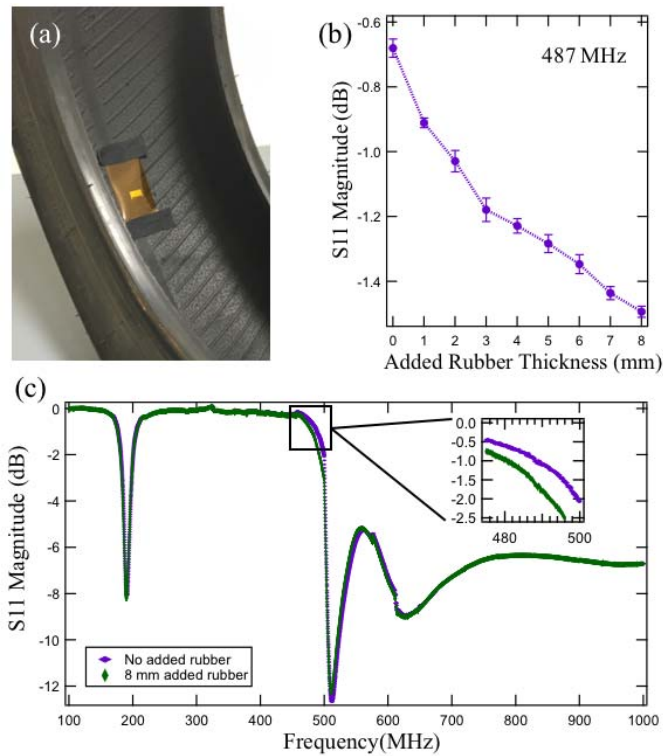


Fig. 6. Reflected signal tests for added rubber thickness on an automobile tire carried out using a vector network analyzer. The sensor was placed on the inner liner of a ~ 1.5 cm thick tire and 1 mm plies of rubber were added on top of the tire tread (corresponding to the sensor's location) to simulate changes in tread depth. A photograph of the sensor is shown in (a). The reflected signal magnitude was taken at 487 MHz, near the resonant frequency. Ten tests were done at each added rubber thickness and 99% confidence intervals are shown in plot (b). A complete sweep from 100 MHz to 1 GHz for both 0 mm of added rubber and 8 mm of added rubber are shown in (c), with an inset of the plot zoomed at the most sensitive frequency.

therefore an operating frequency directly below this resonant frequency was chosen for the data extraction and analysis. This has an added benefit that current tire pressure monitoring systems (TPMS) send pressure data from tires at 433 MHz, making the operation of these tire tread depth sensors readily adaptable to the current TPMS platform.

This proof-of-concept experiment provides reinforcement to the applicability of these noninvasive material thickness sensors and demonstrates a different measurement technique to allow sensing despite the steel mesh in a car tire.

IV. CONCLUSION

In conclusion, we have developed a capacitive-based sensor for noninvasive material thickness detection using fully printed, adjacent electrode structures. We have explored several variables to gain insight into the mechanism behind the sensing, which is the perturbation of electric field propagating between the electrodes due to the overlaid material medium. The m-CNT ink enhances the sensitivity and consistency of the material thickness sensors due to extraordinary surface area-to-volume ratio, quantum-confined electrons, and ultra-thin printed profile. Visual evidence of the perturbation in the fringing electric field lines is shown using COMSOL simulations. We also showed a proof-of-concept with the

sensors noninvasively measuring the tread depth on an automobile tire by being integrated within the tire. These new sensors provide a way to monitor the thickness of a material in a noninvasive fashion with electrically transduced signals, having applicability to a variety of IoT systems.

REFERENCES

- [1] K. Chen *et al.*, "Printed carbon nanotube electronics and sensor systems," *Adv. Mater.*, vol. 28, no. 22, pp. 4397–4414, 2016.
- [2] A. Nathan *et al.*, "Flexible electronics: The next ubiquitous platform," *Proc. IEEE*, Special Centennial Issue, vol. 100, pp. 1486–1517, May 2012.
- [3] S. Harada, W. Honda, T. Arie, S. Akita, and K. Takei, "Fully printed, highly sensitive multifunctional artificial electronic whisker arrays integrated with strain and temperature sensors," *ACS Nano*, vol. 8, no. 4, pp. 3921–3927, 2014.
- [4] S. Yao and Y. Zhu, "Wearable multifunctional sensors using printed stretchable conductors made of silver nanowires," *Nanoscale*, vol. 6, no. 4, pp. 2345–2352, 2014.
- [5] Y. Jung *et al.*, "Fully printed flexible and disposable wireless cyclic voltammetry tag," *Sci. Rep.*, vol. 5, pp. 1–6, Jan. 2015. Art. no. 8105.
- [6] H. Andersson *et al.*, "Investigation of humidity sensor effect in silver nanoparticle ink sensors printed on paper," *IEEE Sensors J.*, vol. 14, no. 3, pp. 623–628, Mar. 2014.
- [7] S. Khan, S. Tinku, L. Lorenzelli, and R. D. Dahiya, "Flexible tactile sensors using screen-printed P(VDF-TrFE) and MWCNT/PDMS composites," *IEEE Sensors J.*, vol. 15, no. 6, pp. 3146–3155, Jun. 2015.
- [8] R. Liu, H. Ding, J. Lin, F. Shen, Z. Cui, and T. Zhang, "Fabrication of platinum-decorated single-walled carbon nanotube based hydrogen sensors by aerosol jet printing," *Nanotechnology*, vol. 23, no. 50, p. 505301, 2012.
- [9] A. D. Franklin, "Nanomaterials in transistors: From high-performance to thin-film applications," *Science*, vol. 349, no. 6249, p. 2750, 2015.
- [10] E. B. Secor and M. C. Hersam, "Emerging carbon and post-carbon nanomaterial inks for printed electronics," *J. Phys. Chem. Lett.*, vol. 6, no. 4, pp. 620–626, 2015.
- [11] E. B. Secor, B. Y. Ahn, T. Z. Gao, J. A. Lewis, and M. C. Hersam, "Rapid and versatile photonic annealing of graphene inks for flexible printed electronics," *Adv. Mater.*, vol. 27, no. 42, pp. 6683–6688, Nov. 2015.
- [12] C. Cao, J. B. Andrews, A. Kumar, and A. D. Franklin, "Improving contact interfaces in fully printed carbon nanotube thin-film transistors," *ACS Nano*, vol. 10, no. 5, pp. 5221–5229, 2016.
- [13] J. Vaillancourt *et al.*, "All ink-jet-printed carbon nanotube thin-film transistor on a polyimide substrate with an ultrahigh operating frequency of over 5 GHz," *Appl. Phys. Lett.*, vol. 93, no. 24, p. 243301, 2008.
- [14] M. Ha *et al.*, "Printed, sub-3V digital circuits on plastic from aqueous carbon nanotube inks," *ACS Nano*, vol. 4, no. 8, pp. 4388–4395, 2010.
- [15] M. F. L. De Volder, S. H. Tawfik, R. H. Baughman, and A. J. Hart, "Carbon nanotubes: Present and future commercial applications," *Science*, vol. 339, no. 6119, pp. 535–539, 2013.
- [16] A. Southard, V. Sangwan, J. Cheng, E. D. Williams, and M. S. Fuhrer, "Solution-processed single walled carbon nanotube electrodes for organic thin-film transistors," *Organic Electron.*, vol. 10, no. 8, pp. 1556–1561, 2009.
- [17] G. J. Brady, Y. Joo, M.-Y. Wu, M. J. Shea, P. Gopalan, and M. S. Arnold, "Polyfluorene-sorted, carbon nanotube array field-effect transistors with increased current density and high on/off ratio," *ACS Nano*, vol. 8, no. 11, pp. 11614–11621, 2014.
- [18] J. W. G. Wilder, L. C. Venema, A. G. Rinzler, R. E. Smalley, and C. Dekker, "Electronic structure of atomically resolved carbon nanotubes," *Nature*, vol. 391, no. 6662, pp. 59–62, 1998.
- [19] H. Mansoor, H. Zeng, and M. Chiao, "Real-time thickness measurement of biological tissues using a microfabricated magnetically-driven lens actuator," *Biomed. Microdevices*, vol. 13, no. 4, pp. 641–649, Aug. 2011.
- [20] M. M. Black, "A modified radiographic method for measuring skin thickness," *Brit. J. Dermatol.*, vol. 81, no. 9, pp. 661–666, 1969.
- [21] C. Arens, D. Reußner, J. Woenkhaus, A. Leunig, C. S. Betz, and H. Glanz, "Indirect fluorescence laryngoscopy in the diagnosis of precancerous and cancerous laryngeal lesions," *Eur. Arch. Oto-Rhino-Laryngol.*, vol. 264, no. 6, pp. 621–626, Jun. 2007.
- [22] E. Sergoyan *et al.*, "Thickness measuring systems and methods using a cavity resonator," U.S. Patent 7 135 869B2, Jul. 21, 2005.

- [23] *Tire-Related Factors in the Pre-Crash Phase*, document DOT HS 811 617, U.S. Department of Transportation, Apr. 2012.
- [24] C. S. Lee and C.-L. Yang, "Thickness and permittivity measurement in multi-layered dielectric structures using complementary split-ring resonators," *IEEE Sensors J.*, vol. 14, no. 3, pp. 695–700, Mar. 2014.
- [25] V. Teodoridis, T. Spicopoulos, and F. E. Gardiol, "The reflection from an open-ended rectangular waveguide terminated by a layered dielectric medium," *IEEE Trans. Microw. Theory Techn.*, vol. 33, no. 5, pp. 359–366, May 1985.
- [26] S. I. Ganchev, N. Qaddoumi, S. Bakhtiari, and R. Zoughi, "Calibration and measurement of dielectric properties of finite thickness composite sheets with open-ended coaxial sensors," *IEEE Trans. Instrum. Meas.*, vol. 44, no. 6, pp. 1023–1029, Dec. 1995.
- [27] *Aerosol Jet 300 Series Datasheet*, Optomec, Albuquerque, NM, USA, Feb. 2016.
- [28] S. Gong *et al.*, "A wearable and highly sensitive pressure sensor with ultrathin gold nanowires," *Nature Commun.*, vol. 5, pp. 1–8, Feb. 2014, Art. no. 3132.



Joseph B. Andrews was born in Richmond, VA, in 1992. He received the B.S. degree in electrical engineering from the University of South Carolina in 2015. He is currently pursuing the Ph.D. degree in electrical engineering with Duke University. His current research interests include printed electronic systems and sensors with an emphasis on internet of things and biosensor applications.



able/flexible/stretchable electronics, sensors and medical devices, and the additive manufacturing and modeling of advanced materials. He has been recognized by many awards, such as the ANU Vice Chancellor's Awards, the U.S. National Congress on Computational Mechanics Travel Award, and the Chinese Government Thousand Talent Award for Young Outstanding Scientists.



Martin A. Brooke (SM'07) received the B.E. (Elect.) (Hons.) degree from Auckland University, New Zealand, in 1981, and the M.S. and Ph.D. degrees in electrical engineering from the University of Southern California, in 1984 and 1988, respectively. He has graduated 23 Ph.D. students from his research group. He is currently an Associate Professor of Electrical Engineering at Duke University. He has published more than 120 articles in technical Journals and Proceedings, and articles on his work have appeared in several trade publications. He holds six U.S. patents.



Aaron D. Franklin (M'09–SM'15) received the B.S.E. degree in electrical engineering from Arizona State University in 2004 and the Ph.D. degree in electrical engineering from Purdue University in 2008.

In 2004, he was a Component Design Engineer at Intel Corporation. He was a Research Staff Member with the IBM T. J. Watson Research Center for six years. In 2014, he joined the Department of Electrical and Computer Engineering and the Department of Chemistry, Duke University, as an Associate Professor. His current research interests include nanomaterials in high-performance nanoelectronic devices, nanomaterial inks for low-cost printed electronics, and harnessing nanomaterial sensitivity in bioelectrical systems, cover a broad range of areas, including nanoelectronics, sensors and circuits for Internet-of-Things, low-voltage transistors, electrical energy conversion/storage, and biosensors.

Dr. Franklin was the Technical Program Chair of the 2017 75th Device Research Conference and the Subcommittee Chair of Nano Device Technology of the IEEE International Electron Devices Meeting in 2017. Over the years, he has served on organizing committees of symposia for various meetings of the Materials Research Society, the Applied Physics Society, the American Chemical Society, and the IEEE.